Hindawi
Journal of Nanomaterials
Volume 2018, Article ID 7096195, 11 pages
https://doi.org/10.1155/2018/7096195

Research Article

Structural, Morphological, Optical, and Room Temperature Magnetic Characterization on Pure and Sm-Doped ZnO Nanoparticles

Khalil Badreddine,[1] **I. Kazah**,[1] **M. Rekaby**,[2] **and R. Awad**[1]

[1]*Physics Department, Faculty of Science, Beirut Arab University, Beirut, Lebanon*
[2]*Physics Department, Faculty of Science, Alexandria University, Alexandria, Egypt*

Correspondence should be addressed to Khalil Badreddine; khalil1978july@hotmail.com

Received 22 March 2018; Accepted 29 May 2018; Published 3 July 2018

Academic Editor: Murtaza Bohra

Nano crystalline $Zn_{1-x}Sm_xO$, $(0.00 \le x \le 0.10)$, were prepared by wet chemical coprecipitation method. The effect of samarium doping on the structural, morphological, optical, and magnetic properties of ZnO nanoparticles was examined by X-ray powder diffraction (XRD), Transmission electron microscopy (TEM), Fourier-transform infrared spectroscopy (FTIR), Ultraviolet-visible spectroscopy (UV) and M-H magnetic hysteresis. XRD analysis showed the hexagonal wurtzite structure of ZnO. The absence of Sm_2O_3 as separate phase may be attributed to the complete dissolving of samarium in ZnO lattice. The lattice parameters (a and c) of $Zn_{1-x}Sm_xO$ were calculated and they fluctuated with the increase of Sm doping which indicated that the structure of ZnO was perturbed by the doping of Sm. The crystallite size was computed for all the samples using Debye-Scherrer's method. The crystallite size decreased with the increase of Sm doping. TEM micrographs revealed that the size and the shape of the ZnO nanocomposites were changed by modifying the doping level of samarium. FTIR analysis spectrum confirmed the formation of ZnO phase and revealed a peak shift between pure and Sm-doped ZnO. The band gap energy and Urbach energy were calculated for $Zn_{1-x}Sm_xO$, $(0.00 \le x \le 0.10)$. The band energy gaps of pure and Sm doped ZnO samples are in the range 2.6–2.98 eV. M-H hysteresis inspection, at room temperature, showed that the pure ZnO exhibited a ferromagnetic behavior incorporated with diamagnetic and paramagnetic contributions. Ferromagnetic behavior was reduced for the doped samples with $x = 0.01$ and $x = 0.04$. The samples with $x = 0.02$ and $0.06 \le x \le 0.10$ tend to be superparamagnetic. The saturation magnetization (M_s), the coercivity (H_c), and the retentivity (M_r) were recorded for $Zn_{1-x}Sm_xO$, $(0.00 \le x \le 0.10)$.

1. Introduction

The unusual physical properties and broad range of applications of semiconductor nanoparticles or quantum dots (QDs) [1, 2], basically II-VI materials, have attracted great attention recently. The phenomenon called "quantum confinement" occurs when the size of the nanocrystals becomes smaller than the corresponding Bohr radius of the exciton. Consequently, the band gap increases and discrete energy levels exist at the edges of the valence and conduction bands [3, 4]. Among the II-VI semiconductors, zinc oxide (ZnO) is very promising due to its essential uses in many research domains. ZnO semiconductor exhibits electronic properties as large exciton binding energy of 60 meV with direct band gap of 3.37 eV [5, 6]. It is nontoxic, cheap, biosafe, and biocompatible [7]. Zinc oxide is a transparent electro conductive material, ultraviolet absorber, and antibacterial agent. Owing to their electrical, optical, mechanical, and magnetic properties resulting from quantum confinement effects, nanoparticles of ZnO are candidates of applications in piezoelectric transducers, transparent field-effect transistors, gas sensors, optical waveguides, transparent conductive films, ultraviolet nanolasers, varistors, photodetectors, solar cells, blue and ultraviolet (UV) optical devices, and bulk acoustic wave devices [8–13]. The modification of metal oxide nanoparticles by doping with special metal and nonmetal elements makes it possible to enhance the electrical and optical properties of materials by changing the surface properties. Doping

semiconductor nanocrystals with transition metals (TMs) forms diluted magnetic semiconductors (DMSs) [14–18]. A vital characteristic of ZnO is the presence of intrinsic defects. The optical, electronic, and magnetic characteristics of ZnO can be modified by doping or the formed intrinsic lattice defects. Recently, room temperature ferromagnetism in ZnO doped with TMs has been studied both theoretically and experimentally [19–21]. ZnO-based DMSs attracted more attention in spintronic applications and optoelectronic devices [22–24]. Doping ZnO nanocrystals with rare earth (RE) ions [25, 26] is identified as candidates for luminescence centers via their optical advantages and in improving the magnetic properties of ZnO. Among the rare earth elements, samarium has allured recognition because of its prospective in different applications. We will briefly introduce some previous studies regarding rare earth and transition element-doped ZnO. Liu et al. [27] integrated Nd^{3+} ions into hexagonal ZnO nanocrystals. Karthikeyan et al. [28] studied the optical properties of ZnO nanoparticles doped by Dy^{3+}. Oprea et al. [29] reported the influence of Gd^{3+} doping on the photoluminescence, magnetic properties, and photocatalytic activity of ZnO nanoparticles synthesized by simple sol-gel method. The optical and magnetic properties in the Eu^{3+}-doped ZnO nanocrystals were reported by Yoon et al. [30]. Using coprecipitation method, Lotey et al. [31] investigated the room temperature ferromagnetism in ZnO nanoparticles when doped by Tb^{3+}. Sekhar et al. [32] researched the effect of Sm^{3+} doping on the structural, optical, and magnetic properties of ZnO nanopowders using the chemical refluxing technique. Farhat et al. [33] reported the influence of Er^{3+} doping on ZnO nanoparticles prepared by wet chemical coprecipitation method. By coprecipitation technique, Sharrouf et al. [34] investigated the result of Mn^{2+} doping on ZnO nanoparticles.

Out of the various techniques that were used for the synthesis of undoped and doped ZnO nanoparticles, coprecipitation is one of the most important techniques in preparing metal-oxide nanoparticles that are highly reactive at low temperature sintering. Within the coprecipitation synthesis technique, the particle size can be controlled by adjusting the pH value using inorganic base, the temperature of the reaction, the annealing temperature, and time [35]. The present work reports the effect of Sm doping with different concentrations up to 10% on the structural, morphological, optical, and magnetic properties of the ZnO nanoparticles. The aim of this work is to reach better results regarding optical and magnetic properties for their importance in luminescence centers and spintronic devices, respectively. The ZnO/Sm nanoparticles were prepared by coprecipitation technique that provides nanopowders with good quality despite of the low cost and simplicity of this method.

2. Materials and Methods

2.1. Preparation of ZnO Nanoparticles. The $Zn_{1-x}Sm_xO$ nanopowders ($x = 0.00$, 0.01, 0.02, 0.04, 0.06, 0.08, and 0.10) were synthesized by coprecipitation technique using zinc chloride as the source of zinc and samarium (III) chloride hexahydrate as the source of dopants. Pure ZnO nanoparticles were prepared by considering 0.2 M zinc chloride ($ZnCl_2$) and an alkali solution of 4.0 M sodium hydroxide (NaOH of pH = 13.8). The solution was prepared by adding 20 g of zinc chloride and 3.72 g of Edta disodium dehydrate into 146.735 ml of purified water. 16 g of NaOH was added to 100 ml of distilled water then added dropwise to the above solution under magnetic stirring for 2 hours at 60°C. The final pH of the solution is ≈12, because a highly basic condition is convenient for the direct preparation of wurtzite-type ZnO crystals to reduce the respective zinc salt and vigorous synthetic environment [36]. The precipitate was separated from the mixture by filtration where it was washed with purified water until pH ≈ 7 and then dried at 100°C for 18 hours. The dried ingots were calcined using the muffle furnace (Gallenkamp FSL-340) at 500°C for 5 hours. Doped Sm-ZnO nanoparticles were synthesized by a similar process except that the used amount of samarium (III) chloride hexahydrate was dependent on the needed concentration of Sm relative to Zn.

2.2. Characterization Methods. The synthesized $Zn_{1-x}Sm_xO$ nanoparticles were characterized by X-ray powder diffraction at room temperature using Bruker D8 advance powder diffractometer with Cu-K_α radiation ($\lambda = 1.54056$ Å) in the range $10^\circ \le 2\theta \le 80^\circ$. TEM micrographs were obtained by using JEOL transmission electron microscope JEM-100CX operated at 80 kV. The FTIR spectra of the powder samples were displayed using FTIR Nicolet iS5-Thermoscientific where about 5 mg of the $Zn_{1-x}Sm_xO$ powder were mixed with 100 mg of KBr and then pressed to form a disk of 0.6 mm thickness and 1.3 cm diameter. UV-visible measurements were recorded, at room temperature, using the ultraviolet-visible-near infrared (NIR) spectrophotometer V-670 that registered the absorption spectra at a range of wavelengths of 190–2500 nm where 5 mg of $Zn_{1-x}Sm_xO$ powder was dissolved in 50 ml of ethanol. Magnetic measurements were performed at room temperature using a vibrating sample magnetometer (Lake Shore 7410) having temperature range capability from 4.2 K to 1273 K.

3. Results and Discussion

3.1. Structure and Morphology. Figure 1 shows the XRD patterns of $Zn_{1-x}Sm_xO$ for $0.00 \le x \le 0.10$. The diffraction peaks belong to the planes (100), (002), (101), (102), (110), (103), (200), (112), (201), and (202). All of the observed peaks harmonized with those of wurtzite hexagonal structure ZnO (JCPDS card number 36-1451, $a = b = 3.249$ Å, $c = 5.206$ Å) with the preferred orientation of (101) planes and no additional peaks appeared for secondary phases that may originate from Sm doping, revealing the good synthesis of ZnO : Sm nanoparticles. The nonexistence of Sm_2O_3 as separate phase may be attributed to the complete dissolving of samarium in ZnO lattice [37]. The diffraction peaks are sharp and narrow, showing the high crystallinity and purity of the synthesized nanoparticles as reported by Ramimoghadam et al. [38] for ZnO nanoparticles prepared using palm olein as biotemplate.

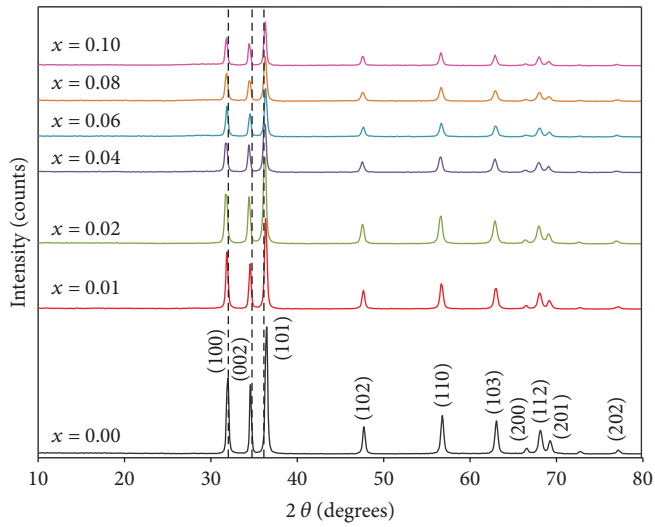

Figure 1: XRD patterns of $Zn_{1-x}Sm_xO$ for $0.01 \le x \le 0.10$.

In Sm-doped ZnO, the diffraction angle (2θ) for the first three peaks showed a slight shift towards lower angles corresponding to pure ZnO sample, and this result was reported by Sekhar et al. [32]. This phenomenon can be interpreted to the difference in the ionic radius of Sm^{3+} (0.95 Å) and Zn^{2+} (0.74 Å). The result of shifted position peaks ensures that the Sm^{3+} ions substituted Zn^{2+} ions in the ZnO matrix and consequently a change in the average of crystal size.

The lattice parameters (a and c) and the unit cell volume (V) of $Zn_{1-x}Sm_xO$ nanoparticles, ($0.00 \le x \le 0.10$), were calculated using the following equations:

$$\frac{1}{d^2} = \frac{4}{3}\left(\frac{h^2 + hk + k^2}{a^2}\right) + \frac{l^2}{c^2}, \quad (1)$$

$$V = \frac{\sqrt{3}}{2}a^2 c, \quad (2)$$

where d is the interplanar distance and (h, k, and l) are the Miller indices.

The average crystallite sizes of the synthesized samples were calculated from XRD spectra using Debye-Scherrer's equation:

$$D = \frac{0.9\lambda}{\beta \cos\theta}, \quad (3)$$

where D is the average crystallite size of the particle, λ is the incident X-ray wavelength, β is the angular peak width at half maximum in radians, and θ is the Bragg's diffraction angle. The calculated lattice parameters, the ratio c/a, the unit cell volume (V), and the average crystallite size (D) of the synthesized samples are listed in Table 1. The crystallite size calculated from XRD was found to decrease with the increase of Sm doping which can be attributed to the intervention of Sm^{3+} in the ZnO crystal growth. The influence of this intrusion can be related with the distortion of the crystal lattice as a result of substitution with larger ionic radii of Sm^{3+} ions (0.95 Å) compared to Zn^{2+} ions with ionic radii (0.74 Å) [39]. Arora et al. [40] reported Sm-doped ZnO samples with average crystallite sizes ranging from 41 to 37 nm. Wang et al. [41] found that the average crystallite sizes of Sm-doped ZnO samples ranges from 10.5 to 7.5 nm. From Table 1, it is clear that the average crystallite size for the prepared samples ranges from 54 to 33 nm which is much closer to Arora et al.'s [40] findings.

Table 1: Values of the lattice parameters (a and c), the ratio (c/a), the unit cell volume (V), and the crystallite size (D) of $Zn_{1-x}Sm_xO$.

x	a (Å)	c (Å)	c/a	V (Å^3)	$D_{(XRD)}$ (nm)	$D_{(TEM)}$ (nm)
0.00	3.2422	5.1936	1.601	47.27	54.0	49.0
0.01	3.2363	5.1643	1.595	46.84	43.0	38.0
0.02	3.2438	5.1946	1.601	47.33	36.0	33.0
0.04	3.2444	5.1974	1.601	47.38	35.0	31.0
0.06	3.2348	5.1827	1.602	46.96	35.0	30.0
0.08	3.2396	5.1888	1.601	47.16	35.0	29.0
0.10	3.3564	5.3920	1.606	52.60	33.0	27.0

The lattice parameters fluctuated with the increase of Sm doping, which indicates that the structure of ZnO was perturbed by the doping of Sm. The results in Table 1 show that the lattice constants a and c of samarium-doped ZnO nanoparticles were larger than those of pure ZnO for $x = 0.02$, 0.04, and 0.10. On the other hand, the lattice parameters decreased for $x = 0.01$, 0.06, and 0.08 relative to pure ZnO. Decrease in lattice parameters is expected when Sm substitutes Zn while the lattice parameter will increase when Sm occupies interstitial sites [42]. The ratio (c/a) is approximately 1.60 for all samples which is compatible with the ideal value for hexagonal cell ($c/a = 1.633$) [43].

Figures 2(a)–2(d) show the TEM micrographs of $Zn_{1-x}Sm_xO$ nanoparticles for $x = 0.00$, $x = 0.01$, $x = 0.06$, and $x = 0.10$, respectively. The size of the particles was

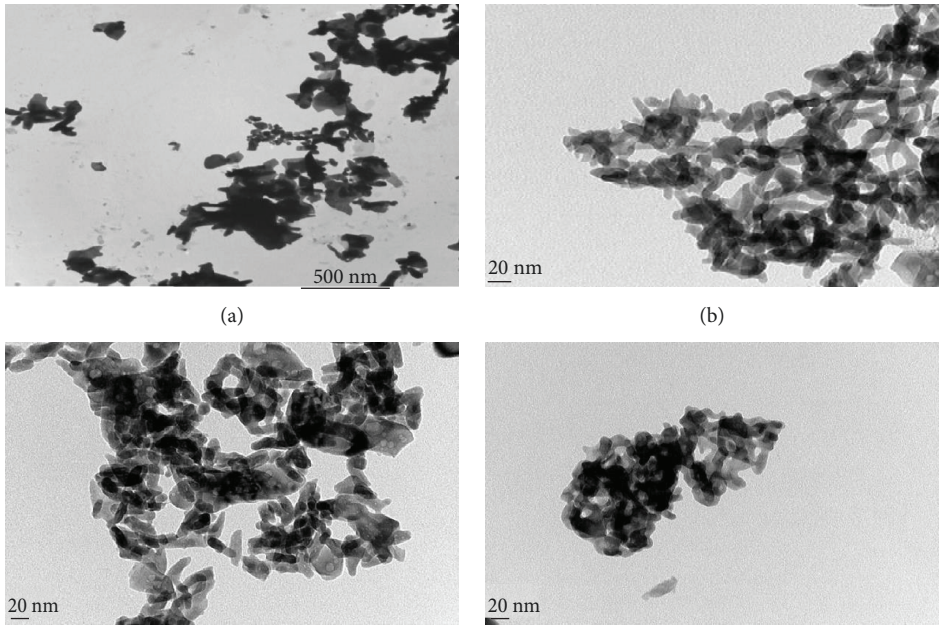

FIGURE 2: TEM micrographs for $Zn_{1-x}Sm_xO$ with (a) $x = 0.00$, (b) $x = 0.01$, (c) $x = 0.06$, and (d) $x = 0.10$.

measured and showed a similar decreasing trend as the crystallite size obtained by XRD measurements with the increase in Sm content. The results are given in Table 1. The particles did not exhibit definite shape for the investigated samples with $x = 0.00$ and $x = 0.10$ which was interpreted by Vaseem et al. [44] that when the reaction is accomplished in dry air, the synthesized ZnO nanoparticles have absence of defined shape or size. The high temperature heating process [45] explains the lack of definite shape, which indicates that destruction in recrystallization of ZnO lattice happened. The particle's shape was modified to nanolike rods for samples with $0.01 \leq x \leq 0.08$ due to the doping level of samarium that results in the alter of the nanoparticle's form [34]. Figure 2(d) shows an agglomeration of the synthesized nanoparticles when the doping level of samarium reaches a concentration of $x = 0.10$.

3.2. Atomic Bonding Vibration Mode Analysis. The composition and quality of the prepared samples were investigated by the FTIR spectroscopy. Figure 3 shows the FTIR spectra of pure and samarium-doped ZnO nanoparticles with $x = 0.00$, 0.04, 0.06, and 0.10. Magnified positions of the first absorption band of $Zn_{1-x}Sm_xO$ samples for $x = 0.00$, 0.04, 0.06, and 0.10 are revealed in the inset of Figure 3. The peaks communicating to the vibrational characteristics of ZnO are viewed for the samples in the range [397–431] cm^{-1} which is ascribed to the Zn-O stretching band [46]. The shift of the peak's position in the doped samples relative to the pure one reflects that the Zn-O structure was perturbed by the presence of Sm in its environment. The slight shift in the Zn-O stretching peak might be due to the change in the parameters and the bond properties of Zn perturbed by Sm doping [34]. This result is similar to that obtained in

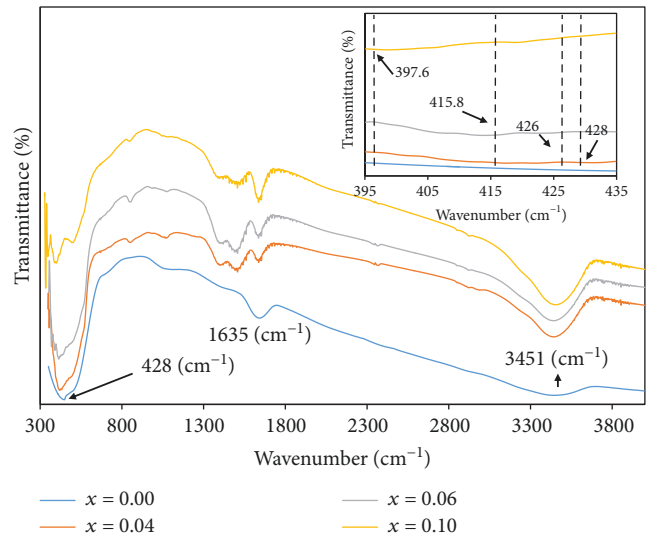

FIGURE 3: FTIR spectra of $Zn_{1-x}Sm_xO$ nanoparticles with $x = 0.00$, $x = 0.04$, $x = 0.06$, and $x = 0.10$. The inset shows the absorption peaks of $Zn_{1-x}Sm_xO$ with $x = 0.00$, $x = 0.04$, $x = 0.06$, and $x = 0.10$ at Zn–O stretching vibration.

Fe-doped ZnO films by Srivastava et al. [47], and it is also explained by Armelao et al. [48] reporting that the stretching modes of ZnO are modified due to the different ionic radii of $Zn^{2+}$and Mn^{2+}. The values of the absorption peak of Zn-O for $0.00 \leq x \leq 0.10$ are listed in Table 2. The peak present at 1635 cm^{-1} is assigned to the OH bending of water, and the broad peak at 3451 cm^{-1} is ascribed to the O-H stretching mode [49]. Presence of O-H group indicates the presence of water molecules on the surface of ZnO nanoparticles even after drying condition in the preparation technique. The

Table 2: Wavelength of Zn-O stretching vibrations.

x	0.00	0.01	0.02	0.04	0.06	0.08	0.10
Wavenumber (cm^{-1})	428.9	431.6	430.4	426.1	415.8	413.6	397.6

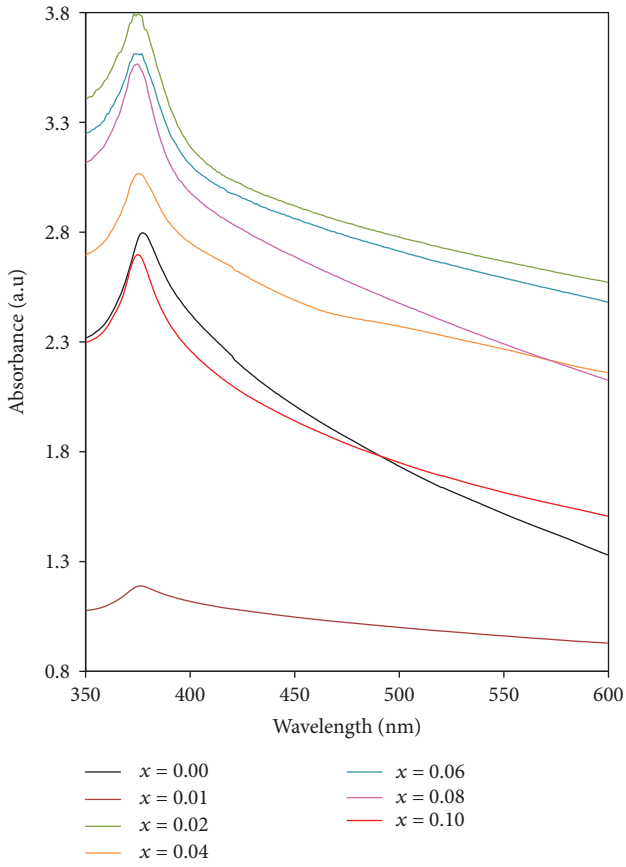

Figure 4: The UV-visible spectroscopy of $Zn_{1-x}Sm_xO$ for $0.01 \le x \le 0.10$.

noticeable bands between 750 cm^{-1} and 1090 cm^{-1} in the synthesized samples may correlate with the bending and twisting modes of vibration of ZnOH. In the range of 1100–1600 cm^{-1}, the absorption peaks could be ascribed to the bending mode of Zn-OH, plane bending of C-OH, and C-OH out-of-plane bending [50].

3.3. Spectrophotometric Measurements of ZnO : Sm Nanoparticles. Figure 4 shows the optical absorption of ZnO : Sm nanoparticles ($0.00 \le x \le 0.10$) which was measured by using the UV-visible optical spectroscopy in a scanning range of wavelength from 350 to 600 nm at room temperature, with scan interval of 1 nm. By the optical absorption result, it is possible to determine each of optical energy band gaps of direct transition occurring in band gap and Urbach energy.

The absorption band edge of undoped ZnO was spotted at 377 nm and it got shifted slightly for the Sm-doped samples which might be attributed to surface effects, modification in the crystallite size, morphology or evidence that the electronic structure of pure ZnO is changed by the doping of samarium [51]. This transposition designates that the Sm ions have incorporated well in the ZnO matrix.

3.3.1. Determination of Optical Energy Band Gap of Direct Transition of ZnO : Sm Nanoparticles. The deviation of the absorption edge, due to doping, explains the change in the energy gap of the prepared samples. The optical band gap of the nanopowders was determined by applying the Tauc relationship as given below [52]:

$$\alpha h\upsilon = C\left(h\upsilon - E_g\right)^n, \tag{4}$$

where α is the absorption coefficient ($\alpha = 2.303A/L$, here A is the absorbance and L is the thickness of the cuvette), C is the constant, h is Planck's constant, υ is the photon frequency, and E_g is the optical band gap. The value of $n = 1/2$, 3/2, 2, or 3 depends on the nature of electronic transition responsible for absorption. Wurtzite ZnO has a direct band gap and $n = 1/2$ in this case.

Figures 5(a) and 5(b) show the graph of $(\alpha h\upsilon)^2$ versus photon energy $h\upsilon$ for ZnO : Sm nanoparticles with $x = 0.00$ and $x = 0.08$. The linear dependences of $(\alpha h\upsilon)^2$ on $h\upsilon$ of ZnO : Sm at higher photon energies reveal that these nanoparticles are essentially direct-transition-type semiconductors. The respective values of E_g for pure and Sm-doped ZnO nanoparticles were obtained by extrapolating to $(\alpha h\upsilon)^2 = 0$. The values of energy band gap are recorded in Table 3 and it was found that the band energy gaps of pure and Sm-doped ZnO samples are in the range 2.6-2.98 eV. The results show that the band gap energy of Sm-doped ZnO nanoparticles with $x = 0.01$ decreased relative to pure ZnO; then, it increased to 2.98 eV for $x = 0.02$. The value of E_g decreased again for $x = 0.04$ then it rose for $0.08 \le x \le 0.10$. Based on the second order perturbation theory, the lowering in E_g may be attributed to *sp-d* interchange interactions and ascribed to *p-d* and *s-d* interactions leading to band gap bowing [51]. Identical results were investigated by Mote et al. [53], Mondal et al. [54], and Singh et al. [55] where the shift in E_g between undoped ZnO and Mn-doped ZnO was found to be 3.26-2.96 eV, 3.22-3.06 eV, and 3.24-3.14 eV, respectively. Recently, Sekhar et al. [32] noticed a decrease in band gap energy of Sm-doped ZnO which was ascribed to the increase in the particle size with increasing Sm concentration. Similar results were recorded by Arora et al. [40] where the decrease in E_g of Sm-doped ZnO was attributed to an increase in the number of defects. Hosseini et al. [56] reported a decrease in E_g of Ag-doped ZnO which was related to the presence of p-type conductivity in the silver-doped ZnO nanoparticles where this reduction in energy gap led to increase the efficiency in the use of these

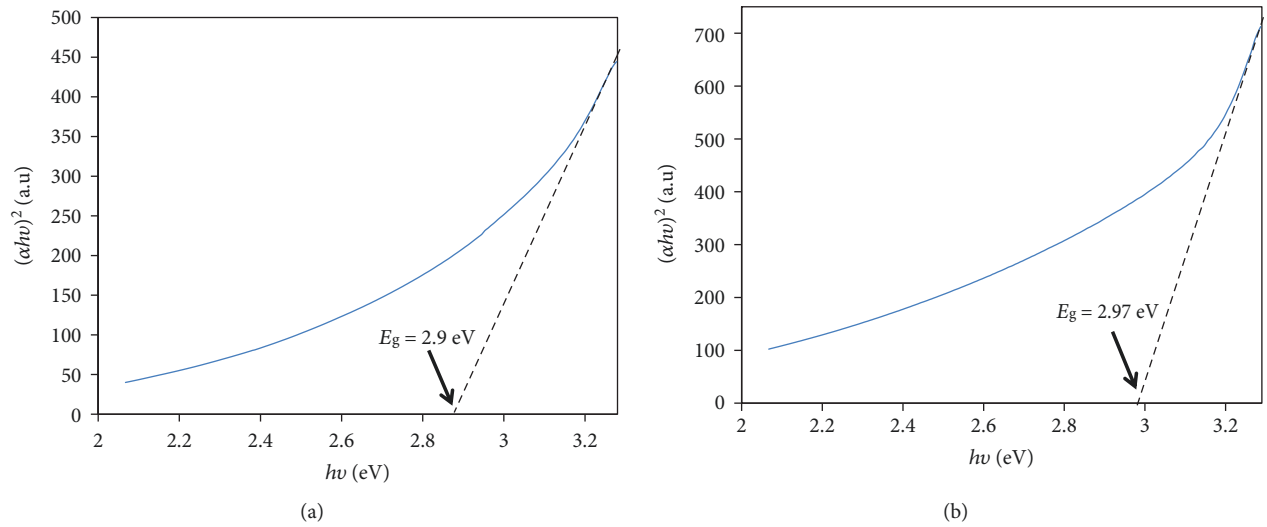

Figure 5: $(\alpha h\upsilon)^2$ versus photon energy $(h\upsilon)$ of $Zn_{1-x}Sm_xO$ for (a) $x = 0.00$ and (b) $x = 0.08$.

Table 3: Values of energy band gap and Urbach energy for $Zn_{1-x}Sm_xO$.

x	E_g (eV)	E_u (eV)
0.00	2.90	2.03
0.01	2.60	6.43
0.02	2.98	4.09
0.04	2.60	4.60
0.06	2.80	4.24
0.08	2.97	3.08
0.10	2.97	2.62

materials in optoelectronic devices. Jayachandraiah et al. [57] interpreted the decrease in E_g to the electron localized states of rare earth activator ion that develop and insert new electronic states nearer to conduction band. Increasing the band gap energy, as a result of quantum confinement effect, is attributed to the reduction in the particle size along with enlarging the doping concentration [39]. Farhat et al. [33] reported that the variation of E_g relies on the particle size and lattice parameters. According to Bras' effective mass model, E_g of nanoparticles can be expressed as a function of particle size as follows:

$$E_g = E_{bulk} + \frac{\hbar^2\pi^2}{2R^2}\left[\frac{1}{m_e} + \frac{1}{m_h}\right] - \frac{1.8\,e^2}{\varepsilon R}, \quad (5)$$

where E_{bulk} is the band gap of the bulk semiconductor, $\hbar$ is the second Plank's constant, R is the radius of the nanoparticle, m_e is the effective mass of the electron, m_h is the effective mass of the hole, e is the charge of electron, and ε is the electric permittivity of the material.

3.3.2. Determination of Urbach Energy of ZnO:Sm Nanoparticles. In the absorption edge, the size of the exponential tail is identified by the Urbach energy which relies on thermal vibrations in the lattice, temperature, average photon energies, static disorder, induced disorder, and on strong ionic bonds. In the low photon energy scale, the spectral dependence of the absorption edge is given by the empirical Urbach rule [58].

$$\propto = \beta e^{h\upsilon/E_u} \quad (6)$$

where β is constant, E_u is the Urbach energy and (υ) is the frequency of the radiation.

The graphs of the logarithm of the absorption coefficient $\ln(\alpha)$ as a function of the photon energy for ZnO:Sm nanoparticles with $x = 0.00$ and $x = 0.08$ are shown in Figures 6(a) and 6(b), respectively. The Urbach energy was determined, in the lower photon energy of these plots, by calculating the reciprocals of the slope of the linear part. The values of E_u are listed in Table 3.

3.4. Magnetic Study. Magnetic behavior of $Zn_{1-x}Sm_xO$ nanoparticles was investigated by tracing, at room temperature, the variation of the magnetization (M) in emu/g as a function of an applied magnetic field (H) as shown in Figures 7(a)–7(d) for the samples with $x = 0.00$, 0.01, 0.08, and 0.10, respectively. The pure ZnO reveals a ferromagnetic behavior. In general, the three possible reasons for ferromagnetism can be summarized as the following: (i) defect related mechanism that is often announced for DMSs [59], (ii) presence of secondary phases of impurities, and (iii) appearance of micro Sm clusters. However, in the present work, the XRD of Sm-doped ZnO nanoparticles did not show indication of secondary phases. Moreover, signs of Sm clusters were not noticed, which display that the samarium atoms successfully replaced the regular Zn sites. In conclusion, the existence of ferromagnetism at room temperature (RTFM) is interpreted by defect-related mechanism. In our samples, the exchange interactions connecting unpaired electron spins emerging from oxygen vacancies along the surface of nanoparticles may be the origin of ferromagnetism. Generally, magnetic semiconducting systems can be

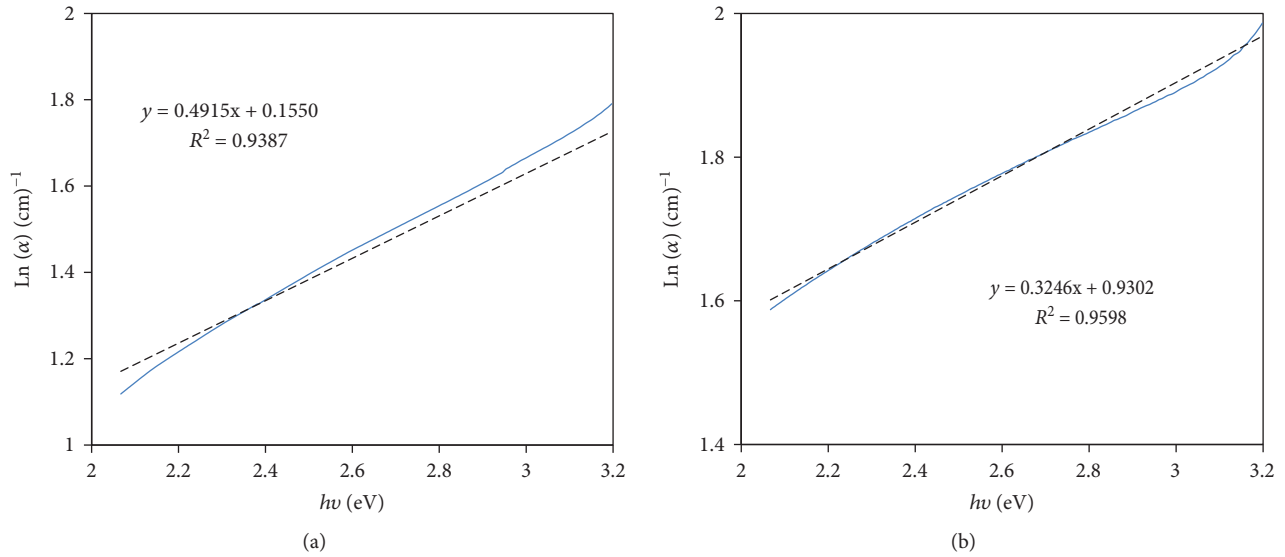

FIGURE 6: ln(α) versus photon energy ($h\upsilon$)is shown in the inset for (a) $x = 0.00$ and (b) $x = 0.08$.

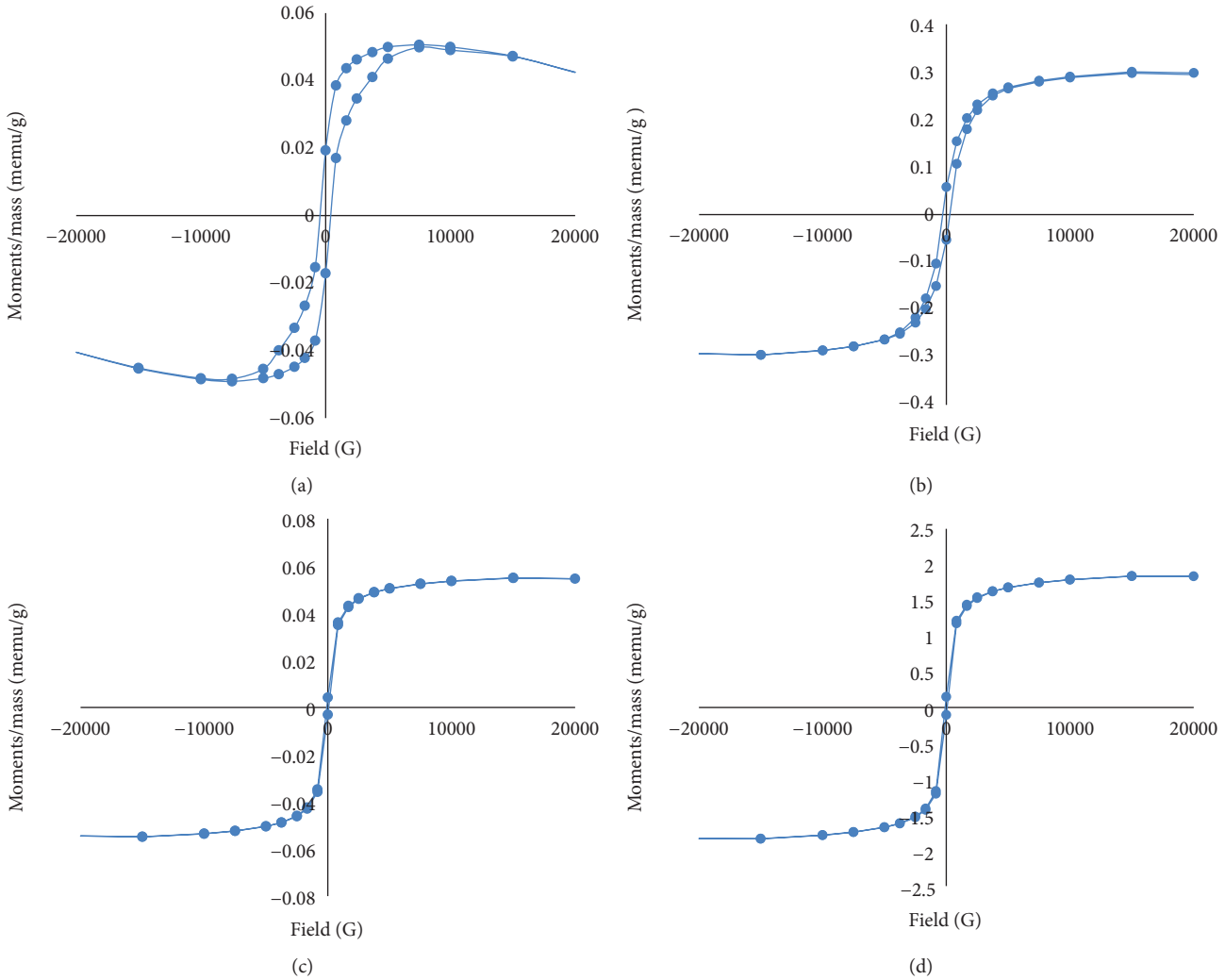

FIGURE 7: (M-H) hysteresis loop of $Zn_{1-x}Sm_xO$ nanoparticles for (a) $x = 0.00$, (b) $x = 0.01$, (c) $x = 0.08$, and (d) $x = 0.10$.

Table 4: The variation of M_s, M_r, H_c, and S as a function of x.

x	M_s (emu/g)	M_r (emu/g)	H_c (G)	$S = M_r/M_s$
0.00	0.0498	0.0182	441.30	0.36546
0.01	0.2970	0.0554	288.36	0.18653
0.02	1.2602	0.0631	61.28	0.05014
0.04	0.3243	0.0050	227.49	0.01541
0.06	1.3665	0.0691	61.54	0.05058
0.08	0.0540	0.0036	78.56	0.06722
0.10	1.8370	0.0001	81.14	0.00006

identified by delocalized band electrons. Magnetic ions are specified by localized 3d or 4f shells. The magnetic properties are determined by the localized magnetic moments accompanied with the magnetic ions and their interaction with the host semiconductor. The interaction accountable for the magnetic behavior is s, p-f in rare earth magnetic ions. Consequently, samarium-doped ZnO shows dilute magnetic semiconducting behavior. The hysteresis loop of undoped ZnO sample also displayed diamagnetic and paramagnetic participations since the magnetization M decreased with the increase of applied magnetic field H after 0.05 G. Phadnis et al. [60] reported similar observations regarding ZnO nanocrystals covered with polyvinyl pyrrolidone (PVP) and prepared by the wet chemical route technique at room temperature.

As the concentration of Sm increased, a serious modification in the magnetic hysteresis loops existed. The RTFM was also observed for the doped samples with concentrations $x = 0.01$ and $x = 0.04$ which may be ascribed to the substitutional inclusion of Sm in Zn-sites. The ferromagnetic nature decreased for these concentrations which may be ascribed to the fact that some Sm atoms approach each other leading to superexchange interactions between them. Thus, RTFM is lowered relative to pure ZnO, and the antiferromagnetic coupling grows in nature.

The hysteresis loops for $x = 0.02$, $x = 0.06$, $x = 0.08$, and $x = 0.10$ are very narrow in comparison with the other samples. Kittel [61] established theoretical predictions regarding energetic stability of a single magnetic domain, determining a critical dimension of a particle (typically nanometers for normal ferromagnets). In smaller particles, existence of a single ferromagnetic zone is favored. Thermal fluctuations acting upon small particles cannot confirm stable bulk magnetization; consequently, the system displays superparamagnetism (SPM) [62]. In accordance with the TEM technique, all synthesized samples have unlike domains of nanoparticle sizes and those for $x = 0.02$ and $0.06 \leq x \leq 0.10$, possess number of particles with sizes smaller than 35 nm that might explain the emergence of superparamagnetism and accordingly smaller contribution to ferromagnetism.

The values of saturation magnetization (M_s), retentivity (M_r), coercivity (H_c) and squareness ratio $S = (M_r/M_s)$ are presented in Table 4.

It can be noticed that the values of M_s and M_r have the same variation trends for $0.00 \leq x \leq 0.08$. The highest value of the saturation magnetization and the lowest value of the retentivity are revealed for $x = 0.10$. The H_c values vary with increasing the doping values. For the samples that showed ferromagnetic behavior with $x = 0.00$, $x = 0.01$ and $x = 0.04$, the values of H_c decreased while the values of M_s increased. Variations in the coercive field were produced by dissimilarity in defect states and anisotropy contribution due to the clusters of crystallites [63]. Jung et al. [64] reported that remanence to saturation ratio ($S = M_r/M_s$) characterizes the squareness of the hysteresis loops, where $S \ll 0.01$ is a typical value for SPM particles. The data of S in our samples are lower than 0.5, denoting that the particles communicate by magnetostatic interaction and the anisotropy decreases in crystal lattice [65, 66]. The squareness ratio (S) of the sample with $x = 0.10$ is 0.00006 which indicates a superparamagnetic behavior.

4. Conclusions

Pure and samarium-doped ZnO nanoparticles ($Zn_{1-x}Sm_xO$), ($0.00 \leq x \leq 0.10$), were prepared by chemical coprecipitation method. XRD investigation revealed the existence of hexagonal wurtzite structure of ZnO with the absence of Sm_2O_3 as separate phase. TEM micrographs revealed that the synthesized particles have no definite shape for $x = 0.00$ and $x = 0.10$ and the form of the particles was modified to nanolike rods for $0.01 \leq x \leq 0.08$. FTIR analysis for pure and doped ZnO samples admitted the existence of O-H and Zn-O stretching modes around 3451 cm^{-1} and 428 cm^{-1}, respectively, with a peak shift regarding Zn-O stretching mode attributed to modifications in parameters and bond properties of ZnO lattice when perturbed by samarium doping. The band gap energies (E_g) and Urbach energies (E_u) were computed from the UV-VIS spectra. The calculated values of E_g were in the range 2.6-2.98 eV. Hysteresis curves from vibrating sample magnetometer study, at room temperature, revealed that undoped ZnO nanoparticles exhibited a ferromagnetic signal merged with diamagnetic and paramagnetic behavior. The ferromagnetism behavior was diminished for the synthesized samples with $x = 0.01$ and $x = 0.04$. A superparamagnetic behavior appeared for samples with $x = 0.02$ and $0.06 \leq x \leq 0.10$ revealing the potential applications in different industries triggering further research. Other parameters such as saturation magnetization, coercive field, and remanent magnetism from VSM analysis were calculated.

Data Availability

The data used to support the findings of this study are included within the article. Any more specific details in the data will be delivered by the corresponding author upon request.

Conflicts of Interest

The authors declare that they do not have conflicts of interest.

Acknowledgments

This work has been performed in the Materials Science Lab, Physics Department, Faculty of Science, Beirut Arab University, Debbieh, in cooperation with the Faculty of Science, Alexandria University, Alexandria, Egypt.

References

[1] V. L. Colvin, M. C. Schlamp, and A. P. Alivisatos, "Light-emitting diodes made from cadmium selenide nanocrystals and a semiconducting polymer," *Nature*, vol. 370, no. 6488, pp. 354–357, 1994.

[2] A. P. Alivisatos, "Perspectives on the physical chemistry of semiconductor nanocrystals," *The Journal of Physical Chemistry*, vol. 100, no. 31, pp. 13226–13239, 1996.

[3] A. A. Bol, R. van Beek, and A. Meijerink, "On the incorporation of trivalent rare earth ions in II–VI semiconductor nanocrystals," *Chemistry of Materials*, vol. 14, no. 3, pp. 1121–1126, 2002.

[4] F. Dejene, A. Ali, H. Swart et al., "Optical properties of ZnO nanoparticles synthesized by varying the sodium hydroxide to zinc acetate molar ratios using a Sol-Gel process," *Open Physics*, vol. 9, no. 5, 2011.

[5] Y. Li, X. Liu, and J. Li, "Preparation and characterization of CeO_2 doped ZnO nano-tubes fluorescent composite," *Journal of Rare Earths*, vol. 28, no. 4, pp. 571–575, 2010.

[6] Y. I. Jung, B. Y. Noh, Y. S. Lee, S. H. Baek, J. H. Kim, and I. K. Park, "Visible emission from Ce-doped ZnO nanorods grown by hydrothermal method without a post thermal annealing process," *Nanoscale Research Letters*, vol. 7, no. 1, p. 43, 2012.

[7] J. Zhou, N. S. Xu, and Z. L. Wang, "Dissolving behavior and stability of ZnO wires in biofluids: a study on biodegradability and biocompatibility of ZnO nanostructures," *Advanced Materials*, vol. 18, no. 18, pp. 2432–2435, 2006.

[8] S. B. Rana, P. Singh, A. K. Sharma, A. W. Carbonari, and R. Dogra, "Synthesis and characterization of pure and doped ZnO nanoparticles," *Journal of Optoelectronics and Advanced Materials*, vol. 12, no. 2, p. 257, 2010.

[9] M. de la L. Olvera and R. Asomoza, "SnO_2 and SnO_2:Pt thin films used as gas sensors," *Sensors and Actuators B: Chemical*, vol. 45, no. 1, pp. 49–53, 1997.

[10] C. R. Gorla, N. W. Emanetoglu, S. Liang et al., "Structural, optical, and surface acoustic wave properties of epitaxial ZnO films grown on (0112) sapphire by metalorganic chemical vapor deposition," *Journal of Applied Physics*, vol. 85, no. 5, pp. 2595–2602, 1999.

[11] K. Nomura, H. Ohta, K. Ueda, T. Kamiya, M. Hirano, and H. Hosono, "Thin-film transistor fabricated in single-crystalline transparent oxide semiconductor," *Science*, vol. 300, no. 5623, pp. 1269–1272, 2003.

[12] M. H. Huang, S. Mao, H. Feick et al., "Room-temperature ultraviolet nanowire nanolasers," *Science*, vol. 292, no. 5523, pp. 1897–1899, 2001.

[13] C. T. Lee, Y. K. Su, and H. M. Wang, "Effect of r.f. sputtering parameters on ZnO films deposited onto GaAs substrates," *Thin Solid Films*, vol. 150, no. 2-3, pp. 283–289, 1987.

[14] J. K. Furdyna, "Diluted magnetic semiconductors," *Journal of Applied Physics*, vol. 64, no. 4, pp. R29–R64, 1988.

[15] J. M. D. Coey, "Dilute magnetic oxides," *Current Opinion in Solid State and Materials Science*, vol. 10, no. 2, pp. 83–92, 2006.

[16] I. Žutić, J. Fabian, and S. Das Sarma, "Spintronics: fundamentals and applications," *Reviews of Modern Physics*, vol. 76, no. 2, pp. 323–410, 2004.

[17] H. Ohno, "Making nonmagnetic semiconductors ferromagnetic," *Science*, vol. 281, no. 5379, pp. 951–956, 1998.

[18] S. A. Wolf, D. D. Awschalom, R. A. Buhrman et al., "Spintronics: a spin-based electronics vision for the future," *Science*, vol. 294, no. 5546, pp. 1488–1495, 2001.

[19] R. G. Hernández, W. L. Pérez, and M. Jairo Arbey Rodríguez, "Electronic structure and magnetism in $Ni_{0.0625}Zn_{0.9375}O$: an ab initio study," *Journal of Magnetism and Magnetic Materials*, vol. 321, no. 17, pp. 2547–2549, 2009.

[20] S. J. Pearton, D. P. Norton, Y. W. Heo et al., "ZnO spintronics and nanowire devices," *Journal of Electronic Materials*, vol. 35, no. 5, pp. 862–868, 2006.

[21] B. Pandey, S. Ghosh, P. Srivastava, D. K. Avasthi, D. Kabiraj, and J. C. Pivin, "Synthesis and characterization of Ni-doped ZnO: a transparent magnetic semiconductor," *Journal of Magnetism and Magnetic Materials*, vol. 320, no. 24, pp. 3347–3351, 2008.

[22] M. Subramanian, P. Thakur, M. Tanemura et al., "Intrinsic ferromagnetism and magnetic anisotropy in Gd-doped ZnO thin films synthesized by pulsed spray pyrolysis method," *Journal of Applied Physics*, vol. 108, no. 5, article 053904, 2010.

[23] M. H. N. Assadi, Y. B. Zhang, P. Photongkam, and S. Li, "Intrinsic ambient ferromagnetism in ZnO:Co induced by Eu codoping," *Journal of Applied Physics*, vol. 109, no. 1, article 013909, 2011.

[24] G. R. Li, X. H. Lu, C. Y. Su, and Y. X. Tong, "Facile synthesis of hierarchical ZnO:Tb^{3+} nanorod bundles and their optical and magnetic properties," *The Journal of Physical Chemistry C*, vol. 112, no. 8, pp. 2927–2933, 2008.

[25] L. Armelao, F. Heigl, A. Jürgensen et al., "X-ray excited optical luminescence studies of ZnO and Eu-doped ZnO nanostructures," *The Journal of Physical Chemistry C*, vol. 111, no. 28, pp. 10194–10200, 2007.

[26] F. J. Duarte, *Tunable Laser Applications*, CRC, New York, NY, USA, 2nd edition, 2009.

[27] Y. Liu, W. Luo, R. Li, and X. Chen, "Optical properties of Nd^{3+} ion-doped ZnO nanocrystals," *Journal of Nanoscience and Nanotechnology*, vol. 10, no. 3, pp. 1871–1876, 2010.

[28] B. Karthikeyan, C. S. Suchand Sandeep, T. Pandiyarajan, P. Venkatesan, and R. Philip, "Spectrally broadened excitonic absorption and enhanced optical nonlinearities in Dy^{3+}-doped ZnO nanoparticles," *Applied Physics A*, vol. 102, no. 1, pp. 115–120, 2011.

[29] O. Oprea, O. R. Vasile, G. Voicu, L. Craciun, and E. Andronescu, "Photoluminescence, magnetic properties and photocatalytic activity of Gd^{3+} doped ZnO nanoparticles," *Digest Journal of Nanomaterials & Biostructures*, vol. 7, no. 4, pp. 1757–1766, 2012.

[30] H. Yoon, J. Hua Wu, J. Hyun Min, J. Sung Lee, J. S. Ju, and Y. Keun Kim, "Magnetic and optical properties of monosized Eu-doped ZnO nanocrystals from nanoemulsion," *Journal of Applied Physics*, vol. 111, no. 7, article 07B523, 2012.

[31] G. S. Lotey, J. Singh, and N. K. Verma, "Room temperature ferromagnetism in Tb-doped ZnO dilute magnetic

semiconducting nanoparticles," *Journal of Materials Science: Materials in Electronics*, vol. 24, no. 9, pp. 3611–3616, 2013.

[32] M. C. Sekhar, U. Chalapthi, V. K. Madhu Smitha, P. T. Poojitha, S. Uthanna, and B. Poornaprakash, "Influence of Sm doping on the structural, optical, and magnetic properties of ZnO nanopowders," *Journal of Superconductivity and Novel Magnetism*, vol. 30, no. 7, pp. 1937–1941, 2017.

[33] S. Farhat, M. Rekaby, and R. Awad, "Synthesis and characterization of Er-doped nano ZnO samples," *Journal of Superconductivity and Novel Magnetism*, pp. 1–11, 2018.

[34] M. Sharrouf, R. Awad, S. Marhaba, and D. El-Said Bakeer, "Structural, optical and room temperature magnetic study of Mn-doped ZnO nanoparticles," *Nano*, vol. 11, no. 4, article 1650042, 2016.

[35] P. Tartaj, M. del Puerto Morales, S. Veintemillas-Verdaguer, T. González-Carreño, and C. J. Serna, "The preparation of magnetic nanoparticles for applications in biomedicine," *Journal of Physics D: Applied Physics*, vol. 36, no. 13, pp. R182–R197, 2003.

[36] A. Naveed Ul Haq, A. Nadhman, I. Ullah, G. Mustafa, M. Yasinzai, and I. Khan, "Synthesis approaches of zinc oxide nanoparticles: the dilemma of ecotoxicity," *Journal of Nanomaterials*, vol. 2017, Article ID 8510342, 14 pages, 2017.

[37] N. R. E. Radwan, "Modification of surface and catalytic properties of Fe_2O_3 due to doping with rare-earth oxides Sm_2O_3 and Y_2O_3," *Applied Catalysis A: General*, vol. 273, no. 1-2, pp. 21–33, 2004.

[38] D. Ramimoghadam, M. Z. B. Hussein, and Y. H. Taufiq-Yap, "Synthesis and characterization of ZnO nanostructures using palm olein as biotemplate," *Chemistry Central Journal*, vol. 7, no. 1, p. 71, 2013.

[39] H. Y. He, J. Fei, and J. Lu, "Sm-doping effect on optical and electrical properties of ZnO films," *Journal of Nanostructure in Chemistry*, vol. 5, no. 2, pp. 169–175, 2015.

[40] D. Arora, K. Asokan, A. Mahajan, H. Kaur, and D. P. Singh, "Structural, optical and magnetic properties of Sm doped ZnO at dilute concentrations," *RSC Advances*, vol. 6, no. 81, pp. 78122–78131, 2016.

[41] Y. Wang, J. Piao, Y. Lu, S. Li, and J. Yi, "Intrinsic ferromagnetism in Sm doped ZnO," *Materials Research Bulletin*, vol. 83, pp. 408–413, 2016.

[42] S. U. Awan, S. K. Hasanain, G. Hassnain Jaffari, D. H. Anjum, and U. S. Qurashi, "Defects induced luminescence and tuning of bandgap energy narrowing in ZnO nanoparticles doped with Li ions," *Journal of Applied Physics*, vol. 116, no. 8, article 083510, 2014.

[43] H. Kim, A. R. M. Yusoff, H. Lee et al., "Effect of ZnO:Cs_2CO_3 on the performance of organic photovoltaics," *Nanoscale Research Letters*, vol. 9, no. 1, p. 323, 2014.

[44] M. Vaseem, A. Umar, and Y. B. Hahn, "ZnO nanoparticles: growth, properties, and applications," in *Metal Oxide Nanostructures and their Applications*, vol. 5, pp. 1–36, American Scientific Publishers, New York, NY, USA, 2010.

[45] N. K. Divya and P. P. Pradyumnan, "Solid state synthesis of erbium doped ZnO with excellent photocatalytic activity and enhanced visible light emission," *Materials Science in Semiconductor Processing*, vol. 41, pp. 428–435, 2016.

[46] R. F. Silva and M. E. D. Zaniquelli, "Morphology of nanometric size particulate aluminium-doped zinc oxide films," *Colloids and Surfaces A: Physicochemical and Engineering Aspects*, vol. 198–200, pp. 551–558, 2002.

[47] A. Srivastava, N. Kumar, and S. Khare, "Enhancement in UV emission and band gap by Fe doping in ZnO thin films," *Opto-Electronics Review*, vol. 22, no. 1, p. 68, 2014.

[48] L. Armelao, M. Fabrizio, S. Gialanella, and F. Zordan, "Sol–gel synthesis and characterisation of ZnO-based nanosystems," *Thin Solid Films*, vol. 394, no. 1-2, pp. 89–95, 2001.

[49] Y. M. Hao, S. Y. Lou, S. M. Zhou, R. J. Yuan, G. Y. Zhu, and N. Li, "Structural, optical, and magnetic studies of manganese-doped zinc oxide hierarchical microspheres by self-assembly of nanoparticles," *Nanoscale Research Letters*, vol. 7, no. 1, p. 100, 2012.

[50] J. Das, I. R. Evans, and D. Khushalani, "Zinc glycolate: a precursor to ZnO," *Inorganic Chemistry*, vol. 48, no. 8, pp. 3508–3510, 2009.

[51] A. Azam, A. S. Ahmed, S. S. Habib, and A. H. Naqvi, "Effect of Mn doping on the structural and optical properties of SnO_2 nanoparticles," *Journal of Alloys and Compounds*, vol. 523, pp. 83–87, 2012.

[52] R. Dogra, A. P. Byrne, and M. C. Ridgway, "PAC investigations of radiation damage annealing in ^{111}In implanted ZnO," *Optical Materials*, vol. 31, no. 10, pp. 1443–1447, 2009.

[53] V. D. Mote, J. S. Dargad, and B. N. Dole, "Effect of Mn doping concentration on structural, morphological and optical studies of ZnO nano-particles," *Nanoscience and Nanoengineering*, vol. 1, no. 2, pp. 116–122, 2013.

[54] S. Mondal, S. R. Bhattacharyya, and P. Mitra, "Preparation of manganese-doped ZnO thin films and their characterization," *Bulletin of Materials Science*, vol. 36, no. 2, pp. 223–229, 2013.

[55] P. Singh, A. Kaushal, and D. Kaur, "Mn-doped ZnO nanocrystalline thin films prepared by ultrasonic spray pyrolysis," *Journal of Alloys and Compounds*, vol. 471, no. 1-2, pp. 11–15, 2009.

[56] S. M. Hosseini, I. A. Sarsari, P. Kameli, and H. Salamati, "Effect of Ag doping on structural, optical, and photocatalytic properties of ZnO nanoparticles," *Journal of Alloys and Compounds*, vol. 640, pp. 408–415, 2015.

[57] C. Jayachandraiah and G. Krishnaiah, "Erbium induced raman studies and dielectric properties of Er-doped ZnO nanoparticles," *Advanced Materials Letters*, vol. 6, no. 8, pp. 743–748, 2015.

[58] M. A. Hassan and C. A. Hogarth, "A study of the structural, electrical and optical properties of copper tellurium oxide glasses," *Journal of Materials Science*, vol. 23, no. 7, pp. 2500–2504, 1988.

[59] B. Panigrahy, M. Aslam, and D. Bahadur, "Effect of Fe doping concentration on optical and magnetic properties of ZnO nanorods," *Nanotechnology*, vol. 23, no. 11, article 115601, 2012.

[60] C. Phadnis, D. Y. Inamdar, I. Dubenko, A. Pathak, N. Ali, and S. Mahamuni, "Ferromagnetic ZnO nanocrystals and Al-induced defects," *Journal of Applied Physics*, vol. 110, no. 11, article 114316, 2011.

[61] C. Kittel, "Domain theory and the dependence of the coercive force of fine ferromagnetic powders on particle size," *Physical Review*, vol. 73, no. 7, pp. 810-811, 1948.

[62] W. Wernsdorfer, R. Clérac, C. Coulon, L. Lecren, and H. Miyasaka, "Quantum nucleation in a single-chain magnet," *Physical Review Letters*, vol. 95, no. 23, article 237203, 2005.

[63] N. Doğan, A. Bingölbali, and L. Arda, "Preparation, structure and magnetic characterization of Ni doped ZnO nano-

particles," *Journal of Magnetism and Magnetic Materials*, vol. 373, pp. 226–230, 2015.

[64] J. S. Jung, L. Malkinski, J. H. Lim et al., "Fabrication and magnetic properties of Co nanostructures in AAO membranes," *Bulletin of the Korean Chemical Society*, vol. 29, no. 4, pp. 758–760, 2008.

[65] S. Xavier, S. Thankachan, B. P. Jacob, and E. M. Mohammed, "Effect of samarium substitution on the structural and magnetic properties of nanocrystalline cobalt ferrite," *Journal of Nanoscience*, vol. 2013, Article ID 524380, 7 pages, 2013.

[66] E. C. Stoner and E. P. Wohlfarth, "A mechanism of magnetic hysteresis in heterogeneous alloys," *Philosophical Transactions of the Royal Society A: Mathematical, Physical and Engineering Sciences*, vol. 240, no. 826, pp. 599–642, 1948.